ISSN 1995-0780, Nanotechnologies in Russia, 2016, Vol. 11, Nos. 9–10, pp. 579–592. © Pleiades Publishing, Ltd., 2016.
Original Russian Text © G.V. Kravchenko, E.N. Domoroshchina, G.M. Kuz'micheva, A.A. Gaynanova, S.V. Amarantov, L.V. Pirutko, A.M. Tsybinsky, N.V. Sadovskaya, E.V. Kopylova, 2016, published in Rossiiskie Nanotekhnologii, 2016, Vol. 11, Nos. 9–10.

Zeolite–Titanium Dioxide Nanocomposites: Preparation, Characterization, and Adsorption Properties

G. V. Kravchenko[a], E. N. Domoroshchina[a], G. M. Kuz'micheva[a]*, A. A. Gaynanova[a], S. V. Amarantov[b], L. V. Pirutko[c], A. M. Tsybinsky[d], N. V. Sadovskaya[e], and E. V. Kopylova[a]

[a] *Moscow Technological University, Moscow, 119454 Russia*
[b] *Federal Scientific Research Center "Crystallography and Photonics," Russian Academy of Sciences, Moscow, 119333 Russia*
[c] *Boreskov Institute of Catalysis, Siberian Branch, Russian Academy of Sciences, Novosibirsk, 630090 Russia*
[d] *Fedorovsky All-Russian Research Institute of Mineral Raw Materials, Moscow, 119017 Russia*
[e] *Karpov Research Institute of Physical Chemistry, Moscow, 105064 Russia*
**e-mail: galina_kuzmicheva@list.ru*

Received February 12, 2016; accepted for publication June 14, 2016

Abstract—Synthesis conditions are optimized to obtain η-phase/zeolite and Hombifine N/zeolite nanocomposites by the modified cold-impregnation method (method 1), which consists of the codispersion of the samples containing the η-phase or Hombifine N with nano-anatase in a dilute KOH solution, and Beta(25) and ZSM-5 zeolites with different modulus, MOR and Y, for the first time, as well as by the TiO_2/zeolite in situ method (method 2), which consists of the addition of zeolites into the reaction mixture during the synthesis of titanium dioxide. The starting components and nanocomposites are characterized by different methods, such as wide- and small-angle X-ray scattering, scanning electron microscopy, and low-temperature nitrogen adsorption (the Brunauer–Emmet–Teller method). The interaction between nanosized titanium dioxide (NTD) and zeolites (except Y) during the formation of the NTD/zeolite nanocomposite (method 2) and the η-phase/MOR nanocomposite (method 1) is revealed, and the presence of NTD in the nanocomposites in nanocrystalline (Hombifine N/zeolite) or amorphous (η-phase/Beta(25) and η-phase/ZSM-5(300)) states is established. It is found that the use of microwave and ultrasonic treatment upon the synthesis of the nanocomposite gives rise to the uniform distribution of spherical particles in the samples; furthermore, they are the same size (η-phase/ZSM-5(12), η-phase/ZSM-5(300), and η-phase/Y) or smaller (η-phase/MOR, η-phase/Beta(25), and η-phase/ZSM-5(40)) when compared to the original η-phase. The size of spherical particles in the η-phase/ZSM-5(40) nanocomposite is comparable with the starting ZSM-5(40) zeolite. It is found that the preparation of nanocomposites by method 2 leads to an increase in the specific surface for the NTD/ZSM-5(12) and NTD/Y nanocomposites and to a decrease in the specific surface for the remaining nanocomposites (most significantly for NTD/MOR) when compared to the zeolite matrix, and promotes the high adsorption capacity of the NTD/zeolite nanocomposites with regard to the extraction of the P(V) ions from the model aqueous system with the maximum value (99.48%) for the NTD/MOR nanocomposite.

DOI: 10.1134/S1995078016050098

INTRODUCTION

Nanocomposites are multicomponent systems consisting of a matrix and nanosized phases (phases), which have a clear phase boundary and varying properties because of differences in their composition and structure. They can show higher property indexes in comparison with each separate component or display fundamentally new properties.

The TiO_2/zeolite nanocomposites should be considered promising materials, each component of which is characterized by a certain set of properties. Zeolites have a large porous specific surface and are typically used as catalysts [1], adsorbents, and agents for water purification and filtration [2–5]. Unique properties of titanium dioxide nanoparticles (NTD) are caused by the formation of surface hydroxyl groups with the high reaction activity upon a decrease in the sizes of crystallites down to 100Å and lower at their concentration in the sample up to 100% [6, 7]. These groups are self-generated in the NTD particles upon contact with water, which gives rise to their resulting high adsorption capacity [6–11]. Owing to the photocatalytic activity of NTD in the ultraviolet part of sunlight [12], high chemical stability, nontoxicity, and low cost, it is a prospective material for the creation of photocatalysts active in the visible spectral range [13, 14].

Table 1. Properties of nanosized titanium dioxide (NTD)

Property	Sample with the η-phase	Hombifine *N* (anatase) [28]
Mean size of crystallites (*D*, nm)	4.0(2)	8.3(4)
Specific surface (S m^2/g; BET/SM)	3.63(4)/3.33	312.8(3.4)/116.4
Size of nanoparticles (*N*, nm)	N_{SM} = 150 N_{BET} = 140 N_{SEM} = 100–250	N_{SM} = 13 N_{SEM} = 10–80
Volume of ultrananopores with a size from 0.4 to 2 nm (cm^3/g)	0.0008	0.083
Volume of nanopores with a size of to 300 nm (cm^3/g)	0.0068	0.349

The NTD/zeolite nanocomposites show photocatalytic properties (PCA) under the influence of UV radiation [15–20] and the nanocomposites modified by Ag(I) ions in the visible range band [21]; they also show adsorption [22, 23] and bactericidal properties [15, 24]. The use of the NTD/zeolite nanocmposites increases the sorption ability upon the extraction of Pb(II), Cu(II), Zn(II), and Cd(II) ions from aqueous solutions of increased acidity (controlled by the addition of a 0.1 mol/dm^3 solution of HNO_3 or NaOH) when compared to the initial zeolites [25]. Moreover, the above properties of the NTD/zeolite nanocomposites depend on the characteristics of both zeolite (for example, an increase in the Si/Al ratio in zeolite composition leads to an increase in the rate of photodegradation of formaldehyde and trichloroethylene in the presence of NTD/Y and NTD/ZSM-5 [26]) and NTD (improvement of photocatalytic and adsorption properties with a decrease in the size of crystallites and an increase in the specific surface [19, 25, 26]).

The properties of the nanocomposites depend not only on the characteristics of their initial components (matrix and functional nanoparticles), but also on their preparation methods. The syntheses of the NTD/zeolite nanocomposites by the sol-gel [15, 16, 18, 19] and ion-exchange [21, 22] methods, by sputtering of NTD on zeolite [23], and mechanical mixing [20, 24] are reported in the literature. NTD with the structure of anatase or of a mixture of anatase with rutile (Evonik Degussa P25 (Aeroxide)) were used as nanoparticles, and the ZSM-5 [15–17, 22], MOR [20], Beta [18], Y [19], X [23], and 5A [27] zeolites were used as a matrix. It was shown in [26] that the impregnation method appears to be more economic in comparison with the method of mechanical mixing due to a significant decrease in the NTD concentration upon the preparation of a nanocomposite, while the rate of photocatalytic transformation remains the same. The impregnation method is one of few environmentally safe processes for the preparation of photocatalysts on the basis of NTD [17].

Despite the existing data on the preparation and properties of some NTD/zeolite nanocomosites, data on the characteristics of NTD and zeolite-based nanocomposites containing it, depending on their preparation methods and when compared with both each other and the matrix nature, are absent in the literature.

The aims of the present studies are the development of the methods for the preparation of NTD/zeolite nanocomposites, their characterization, and investigation of the adsorption properties. The Beta (25), MOR, Y and ZSM-5 (12), ZSM-5 (40), and ZSM-5 (300) zeolites are chosen as a matrix, and commercial Hombifine N (Sigma-Aldrich) with nano-anatase and its η-modified samples are chosen as functional nanoparticles.

The extension of the range of characterized nanocomposites by using different modifications of nanosized titanium dioxide and zeolites of different natures makes it possible to reveal the compositions most promising for practical applications.

EXPERIMENTAL

Materials

The NTD/zeolite nanocomposites where NTD is nanosized titanium dioxide (Hombifine N commercially available from Sigma-Aldrich) or the sample with the η-phase (Table 1) and zeolites is Beta (25), MOR, Y and ZSM-5 (12), ZSM-5 (40), or ZSM-5 (300) (Table 2) are studied.

Synthesis of Nanocomposites and Physicochemical Methods

The NTD/zeolite nanocomposites were synthesized by the two following methods.

Method 1 (modified method of cold impregnation) consists of the mixing of samples containing NTD (Hombifine N or a sample with the η-phase) with zeolites; their co-dispersion in a dilute KOH solution (pH ~ 8); subsequent stirring at room temperature together with the ultrasound treatment (UST) in the case of the η-phase/ZSM-5 (40), Hombifine N/ZSM-5 (40), η-phase/MOR, Hombifine N/MOR, Hombifine N/ZSM-5 (12), and η-phase/ZSM-5 (12) nanocomposites; or microwave treatment (MWT) in the case of the η-phase/Beta (25), Hombifine N/Beta (25),

Table 2. Properties of zeolites

Zeolite (brand-name)	Structural type	System of channels (dimensionality; diameter, Å; cross section, Å)	Si/Al (zeolite modulus)	Microstructure characteristics		Space group	Chemical composition	Morphology (SEM data)
				V_Σ, cm^3/g	S_{BET}, m^2/g			
Beta (25)	BEA	3 7.6 × 6.4 5.5 × 5.5	25	0.403*	640–680*/399.5**	$P4_122$	$Na(H)_n[Al_nSi_{64-n}O_{128}](H_2O)_x$, $n < 7$	Fractal spherical formations
ZSM-5 (12)	MFI	3 5.3 × 5.6 5.1 × 5.5	12	0.210*	336–382*/169.8**	Pnma	$Na(H)_n[Al_nSi_{96-n}O_{192}](H_2O)_{16}$, $n < 27$	Faceted prisms and small number of spherical particles
ZSM-5 (40)	MFI	3 5.3 × 5.6 5.1 × 5.5	40	0.264*	386–429*/377.3**			Spherical particles (fractal formations)
ZSM-5 (300)	MFI	3 5.3 × 5.6 5.1 × 5.5	300	0.218*	414*/309.5**			Spherical particles (with a size to 100 nm) and some faceted prisms
MOR	MOR	2 6.5 × 7.0. 2.6 × 5.7	5	0.195-0.200*	–/332.6**	Cmcm	$Na(H)_8[Al_8Si_{40}O_{96}](H_2O)_{24}$	Large faceted particles (bipyramides and squized prisms)
Y	FAU	Cavities 7.4	5	0.371*	509–900*/490.6**	Fd3m	$Na(H)_{58}[Al_{58}Si_{134}O_{384}](H_2O)_{240}$	Hexagones and some faceted bipyramides (elongated octahedrons)

*Literature data.

**Original data, where V_Σ (cm^3/g) is the total volume of pores in zeolite and S_{BET} (m^2/g) is the specific surface according to BET.

η-phase/ZSM-5 (12), Hombifine N/ZSM-5 (12), η-phase/ZSM-5 (300), Hombifine N/ZSM-5 (300), η-phase/Y, and Hombifine N/Y nanocmosites; or without treatment in the case of the Hombifine N/ZSM-5 (12) and η-phase/ZSM-5 (12), followed by separation of a solid phase by vacuum filtration and drying at 90°C (Fig. 1). It should be noted that method 1 in the present work differs from the methods used for the preparation of nanocomposites in [17, 26] by the experimental stages and is easier to accomplish.

Method 2 (the in situ method) consists of the addition of zeolite into the reaction mixture during the synthesis of NTD by the fast hydrolysis of titanyl sulfate at a temperature of 93(±2)°C, in the separation of the obtained solid phase by vacuum filtration, washing it with water and acetone, and drying (Fig. 2).

X-ray diffraction studies of the samples by the method of wide-angle X-ray scattering (WAXS) with rotation were performed on a HZG-4 diffractometer with a flat graphite monochromator (CuK_α radiation on a diffracted X-ray beam in a step-wise mode, the pulse accumulation time was 10 s, the step value was 0.02°, and the 2θ angle interval was in the range from 2 to 50° or to 80°). The qualitative phase analysis of the samples with the studied nanocmposites was performed using the PCPDFWIN PDF-2 database; the quantitative analysis is carried out using the Technol-1 software package [29].

The sizes of NTD crystallites (D, Å) in the initial samples and Hombifine N/ZSM-5 (12) nanocomposites (before and after UST or MWT) are determined from the following formula: $D = 0.9\lambda/\beta\cos\theta$, where λ is the wavelength, $CuK_\alpha = 1.54051$ Å, $2\theta \sim 25°$, and

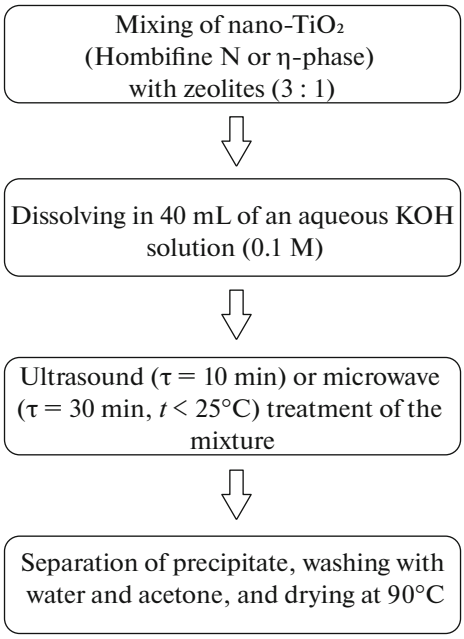

Fig. 1. Synthesis conditions for the NTD/zeolite nanocomposites, where NTD is Hombifine N or the η-phase (method 1).

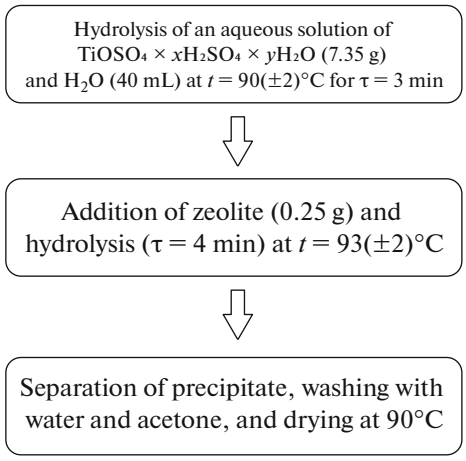

Fig. 2. Synthesis conditions for the NTD/zeolite nanocomposites (method 2).

β is the integrated peak width. The standard deviation is 5%.

X-ray diffraction studies by the method of small-angle X-ray scattering (SAXS) are performed on a HECUS (Austria) laboratory set (the radiation source is an X-ray tube with a copper anode having the characteristic radiation wavelength, $\lambda(CuK_\alpha) = 1.54051$ Å; the operational mode of the X-ray tube corresponds to the voltage, $U = 50$ kV, and the current, $I = 40$ mA; the characteristic radiation line is cut off by a filter of Ni foil with a thickness of 50 μm). The X-ray beam incident on a sample was formed by a Kratky collimator [30]; i.e., slit collimation helped form the hatch-pattern geometry of the X-ray beam on the sample (0.25 × 8 mm) with a sample-detector distance of 267 mm; the scattered radiation was registered by a one-dimensional position-sensitive gas detector. In connection with a nondotted spot formed by the X-ray beam on the sample (0.25 × 8 mm), a collimation correction term was introduced by means of special software tools (so-called operation of the reduction to an ideal instrument). The transition to a scale of the dispersion vector module and the introduction of collimation corrections were carried out with the standard sample (silver behenate) [31].

Scanning electron microscopy (SEM) studies were carried out on a high-resolution JSM 7500F electron microscope using the procedures described in [32].

The sorption capacities of the zeolites and nanocomposites with reference to nitrogen were measured using the standard ASTM D4780-12 procedure (room temperature and vacuum system) by the Brunauer–Emmet–Teller (BET) method from a linear branch of the adsorption isotherm in the area of equilibrium relative pressures of nitrogen (0.05–0.30 P/P_0) [33]. The isotherms obtained for nonporous standard samples of aluminum oxide (0.5 m^2/g and 105 m^2/g under numbers 2003 and 2005, respectively, Quantachrome Instruments) were used as standard. The surface area of micropores ($S_{micropore}$, m^2/g), defined as the total surface area of all deep cracks, crinkles, and pores opened to the surface, and the external surface area of particles ($S_{external}$, m^2/g), defined as the total surface area of all particles in the nanocomposites with reckoning their roughness, were determined from the t-diagram (dependence of the adsorbed gas volume on the adsorptive film thickness, t) [34].

The adsorption properties of the studied samples were measured in an aqueous solution with a phosphorus concentration of 10 mg/L, prepared from the standard P(V) solution (aqueous solution of orthophosphoric acid), at pH = 5.4, a solution volume of 5 mL, an exposure time of 180 min, and a solution temperature of 20°C. The concentration of P(V) in solutions after the sorption (C_{fin}) was measured by the method of atomic emission spectrometry with the inductively coupled plasma (ICPE-9000 Shimadzu, Japan). The P(V) sorption degree ($R_{P(V)}$, %) was calculated by the following formula: $R_{P(V)} = 100[1 - (C_{fin})/(C_{init})]$, %. The standard deviation is 2%.

RESULTS AND DISCUSSION

Synthesis and Characterization

Method 1. The diffractograms of the initial samples with NTD are shown in Figs. 3a and 3b. Hombifine N contains anatase (JCPDS no. 46-1238, diffraction peaks at 2θ of ~25°, ~38°, and ~48°, Fig. 3a). The

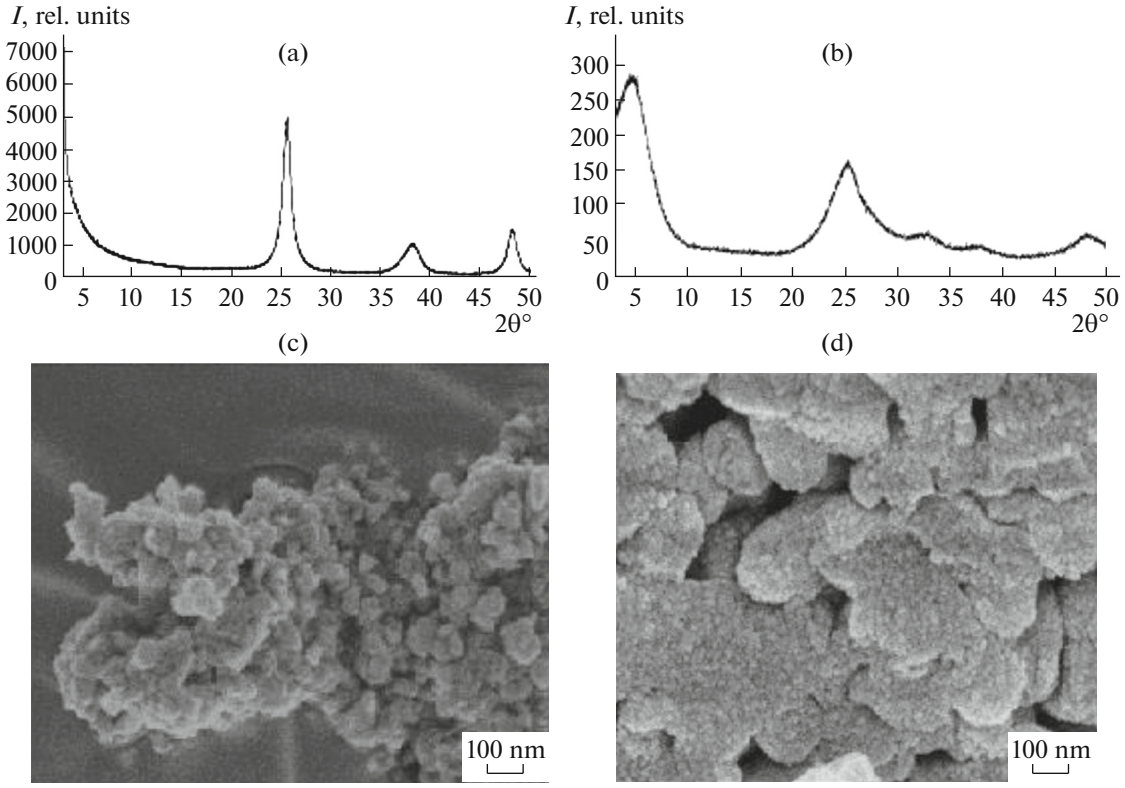

Fig. 3. Diffractograms of initial samples with the (a) Hombifine N and (b) η-phase NTDs and microphotographs of the (c) Hombifine N and (d) η-phase microstructures.

observed reflexes at 2θ of ~5° and ~33° on the diffractogram of the sample with the η-phase obtained by the sulfate method [6, 35] (Fig. 3b) are typical for this phase, while the reflexes at 2θ of ~25° and ~48° correspond to anatase. The η-phase nanoparticles have the formula $TiO_{2-x} \cdot nH_2O$ with a superstructure to the anatase structure; traces of TiO_{2-x}, OH^-, SO_4^{2-} (HSO_4^-), and water are present on their surface [36]. In accordance with the diffraction reflex at 2θ of ~38°, the sample with the η-phase (Fig. 3b) comprised of two phases [6], while the performed quantitative analysis indicates the mixture of anatase (~30%) and the η-phase (~70%).

According to the SEM data, the particle sizes for Hombifine N (N_{SEM} ~ 10–80 nm) (Fig. 3c and Table 1) are less than for the η-phase (N_{SEM} ~ 100–250 nm at $N_{SEM(min)}$ ~ 10 nm) (Fig. 3d and Table 1), and the sizes of crystallites, on the contrary, are larger (D = 8.3(4) nm for Hombifine N, and D = 4.0(2) nm for the η-phase). As is seen from Figs. 3c and 3d, the structure of NTD shows a fractal nature; i.e, the larger formations are composed of smaller particles. Thus, particles in the sample with the η-phase tend to form associates (Fig. 3d).

Based on the analysis and calculation of the diffractograms of the NTD/zeolite nanocomposites (Figs. 4b–9b), it is found that anatase in the samples with Hombifine N is present in the nanosized form, and its content corresponds to the batch concentration (~75%). The amorphous η-phase is detected on the diffractograms of the η-phase/zeolite nanocomposites with Beta (25) (Fig. 4c) and ZSM-5 (300) (Fig. 7c) prepared by applying MWT. NTD is not observed on the diffractograms of the η-phase/MOR nanocomposite prepared by the UST and MWT methods (Figs. 8c, 8d), but this does not exclude different types of interactions of NTD with the MOR zeolite upon the formation of the nanocomposite. NTD in the remaining nanocomposites is present in the amorphous form, as is indicated by the characteristic halo at 2θ of ~25°.

To analyze the influence of the application of UST and MWT during the synthesis of nanocomposites, diffractograms of the η-phase/ZSM-5 (40) and η-phase/MOR nanocomposites prepared with the use of MWT (Figs. 6c and 8c) and UST (Figs. 6d and 8d) are obtained. On the diffractogram of the η-phase/ZSM-5 (40) nanocomposite prepared with the use of MWT, the weak diffraction peaks of zeolite at 2θ of ~27° and ~33° are present, which are absent in the sample prepared with UST (Fig. 6d), and amorphous halo of NTD is observed in both cases. The diffractograms of the η-phase/MOR samples prepared with the use of MWT and UST do not differ basically, except for small increases in the intensity of some peaks of zeolite at 2θ of ~26°, ~27°, and ~31°, in the case of MWT (Fig. 8c)

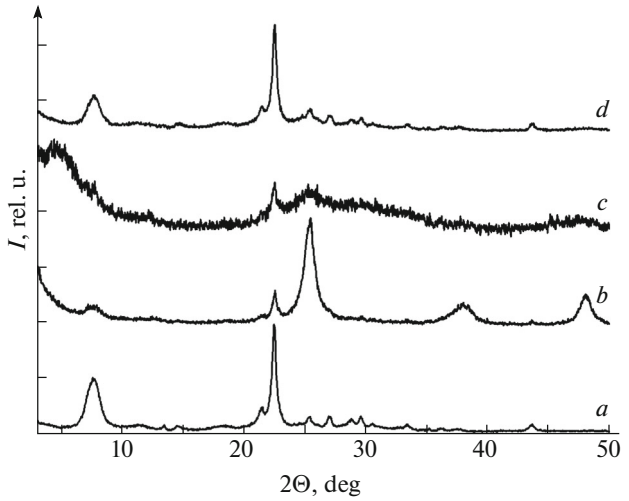

Fig. 4. Diffractograms of the (*a*) Beta(25) zeolite and (*b*) Hombifine N/Beta(25) (MWT), (*c*) η-phase/Beta(25) (MWT, method 1), and (*d*) NTD/Beta(25) (method 2) nanocomposites.

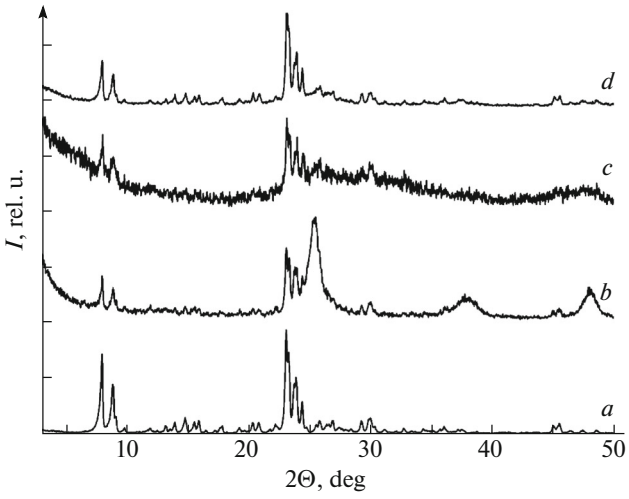

Fig. 5. Diffractograms of the (*a*) initial ZSM-5 (12) zeolite and (*b*) Hombifine N/ZSM-5 (12) (MWT, method 1), (*c*) η-phase/ZSM-5 (12) (MWT, method 1), and (*d*) NTD/ZSM-5 (12) (method 2) nanocomposites.

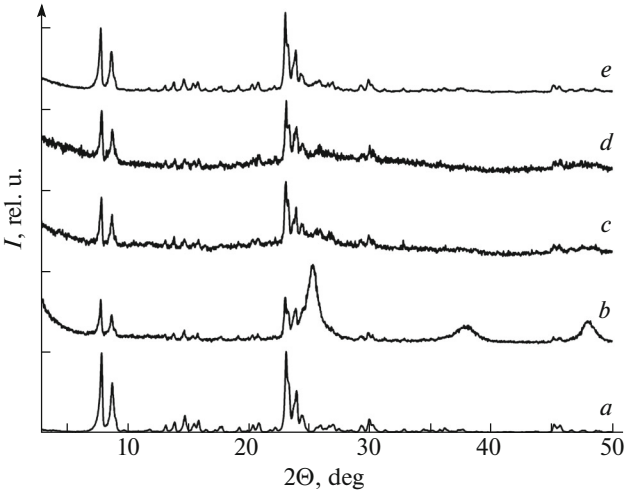

Fig. 6. Diffractograms of the (*a*) initial ZSM-5 (40) zeolite and (*b*) Hombifine N/ZSM-5 (40) (UST, method 1), (*c*) η-phase/ZSM-5 (40) (MWT, method 1), (*d*) η-phase/ZSM-5 (40) (UST, method 1), and (*e*) NTD/ZSM-5 (40) (method 2) nanocomposites.

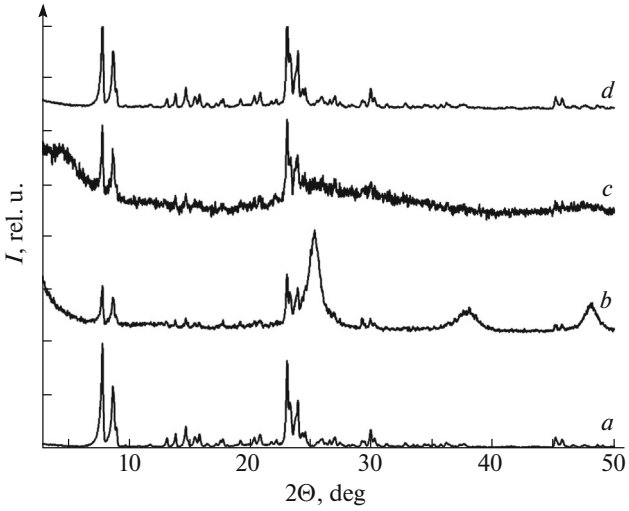

Fig. 7. Diffractograms of the (*a*) initial ZSM-5 (300) zeolite and (*b*) Hombifine N/ZSM-5 (300) (MWT, method 1), (*c*) η-phase/ZSM-5 (300) (MWT, method 1), and (*d*) NTD/ZSM-5 (300) (method 2) nanocomposites.

as compared to the sample prepared with the use of UST (Fig. 8d). These facts indicate a stronger influence of UST on the homogeneity of the formed product.

The morphology of the η-phase/zeolite nanocomposites is characterized by the spherical form of particles (Fig. 12), with the exception of the η-phase/MOR (UST) nanocomposite, in which the faceted forms inherent to the initial zeolite are observed along with spherical particles ($N_{SEM} \leq 100$ nm with $N_{SEM(min)} \sim$ 20 nm, Fig. 12n) of sizes less than the sizes of particles in the initial sample with the η-phase (Table 1, $N_{SEM} \sim$ 100 to 250 nm). It should be noted that this is the only nanocomposite for which the reaction between its initial components (η-phase and MOR zeolite) is supposed (Fig. 8c). The morphology of the nanocomposites prepared by using MWT from the η-phase and ZSM-5 (12) (Fig. 12e, NTD content is 32 to 33 wt % according to X-ray spectral microanalysis) and Y (Fig. 12q, NTD content is about 38 wt %) zeolites is presented by spheres ($N_{SEm} \leq 250$ nm) connected by isthmuses, unlike to the initial zeolites with mainly faceted forms (Table 2; Figs. 12d, 12p). Spherical for-

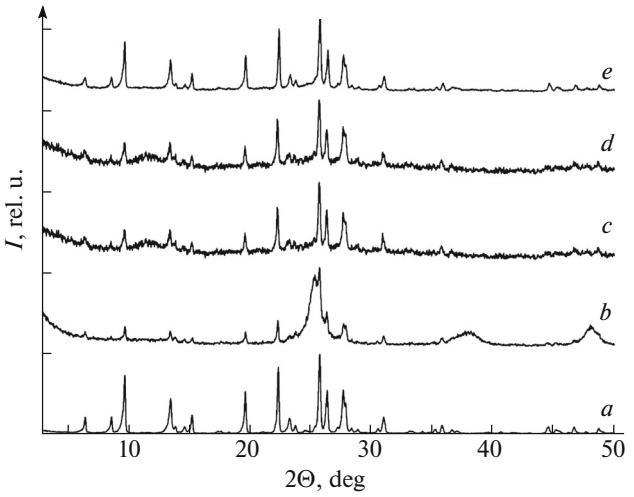

Fig. 8. Diffractograms of (*a*) the initial MOR zeolite and (*b*) Hombifine N/MOR (UST, method 1), (*c*) η-phase/MOR (MWT, method 1), (*d*) η-phase/MOR (UST, method 1), and (*e*) NTD/MOR (method 2) nanocomposites.

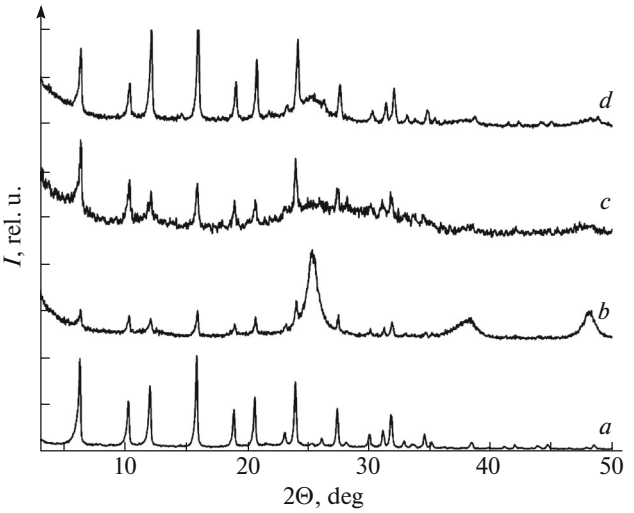

Fig. 9. Diffractograms of the (*a*) initial Y zeolite and (*b*) Hombifine N/Y (MWT, method 1), (*c*) η-phase/Y (MWT, method 1), and (*d*) NTD/Y (method 2) nanocomposites.

mations are revealed also in the photographs of the microstructures of the η-phase/Beta (25) (Fig. 12b, NTD content is from 24 to 61 wt % according to X-ray spectral microanalysis) and η-phase/ZSM-5 (300) (Fig. 12k, NTD content is 3.4 to 34.1 wt % according to X-ray spectral microanalysis) nanocomposites prepared using MWT, with $N_{SEM} \leq 100$ nm and $N_{SEM} \leq 300$ nm, respectively. However, their morphology significantly differs from the morphology of the initial zeolites, which have fractal spherical formations in the case of the Beta (25) zeolite, and both spherical particles and separate faceted prisms in the case of the ZSM-5 (300) zeolite (Table 2). Like in the initial zeolite (Table 1), fractal spherical formations with N_{SEM} in the range from 150 to 1000 nm and smaller particles (≤150 nm) are visible in the photograph of the microstructure of the η-phase/ZSM-5 (40) (UST) nanocomposite (Fig. 12h). The smallest particles in the nanocomposites of the η-phase with the ZSM-5 (12), ZSM-5 (40), and Beta (25) zeolites have the size, $N_{SEM(min)} \sim 20$ nm.

As shown by the example of the Hombifine N/ZSM-5 (12) nanocomposites (Figs. 10a, 10c, 10d), the use of either UST or MWT in the intermediate stage of the synthesis (Fig. 1) exerts the same influence on the mean size of anatase crystallites (D = 8.5(7) nm without treatment, D = 7.7(7) nm with UST, and D = 7.6(6) nm with MWT), which become smaller as compared to initial Hombifine N (D = 8.3(4) nm, Table 1). According to the SEM data (Fig. 10), the elements of the microstructure of the Hombifine N/ZSM-5 (12) nanocomposite sample prepared without any treatment (Fig. 10e) are mainly presented by faceted forms and small amounts of spheres with a size of <350 nm, like in the initial zeolite (Fig. 12d); however, the latter contains spherical particles of smaller sizes (<200 nm), and these sizes are even smaller (<80 nm) in the initial NTD (Table 1). The above indicates the association of small particles into large aggregates in the Hombifine N/ZSM-5 (12) nanocomposite. A similar situation is observed upon using UST (Fig. 10c) or MWT (Fig. 10a) in the intermediate stage of the synthesis; namely, small spherical particles with a size of <100 nm (UST) and <50 nm (MWT) are combined into large particles with a size of <1100 nm (UST, Fig. 10c) and <1250 nm (fractal formations are formed with MWT, Fig. 10a) with the preservation of a small number of faceted forms resembling the particles in the initial ZSM-5 (12) zeolite (MWT, Table 2).

The above statement is confirmed using the example of the application of different kinds of treatments upon the synthesis of the η-phase/ZSM-5 (12) nanocomposites; specifically, the content of spherical particles (<100 nm) in the η-phase/ZSM-5 (12) samples after using UST in the intermediate stage of the (Fig. 10d) increases in comparison with the nanocomposite prepared without treatment (Fig. 10f), while MWT gives rise to the appearance of even larger number of spheres with a size of <100 nm and to their association into larger formations with a size of <700 nm (Fig. 10b).

Thus, both UST and MWT upon their use in the intermediate stage of the synthesis reduce the size of crystallites, increase the number of spherical forms, and promote their association into larger formations. To a greater extent, these phenomena are characteristic for the samples with MWT in which fractal formations are formed. The use of commercial Hombifine N as NTD increases the number of spheres in the nano-

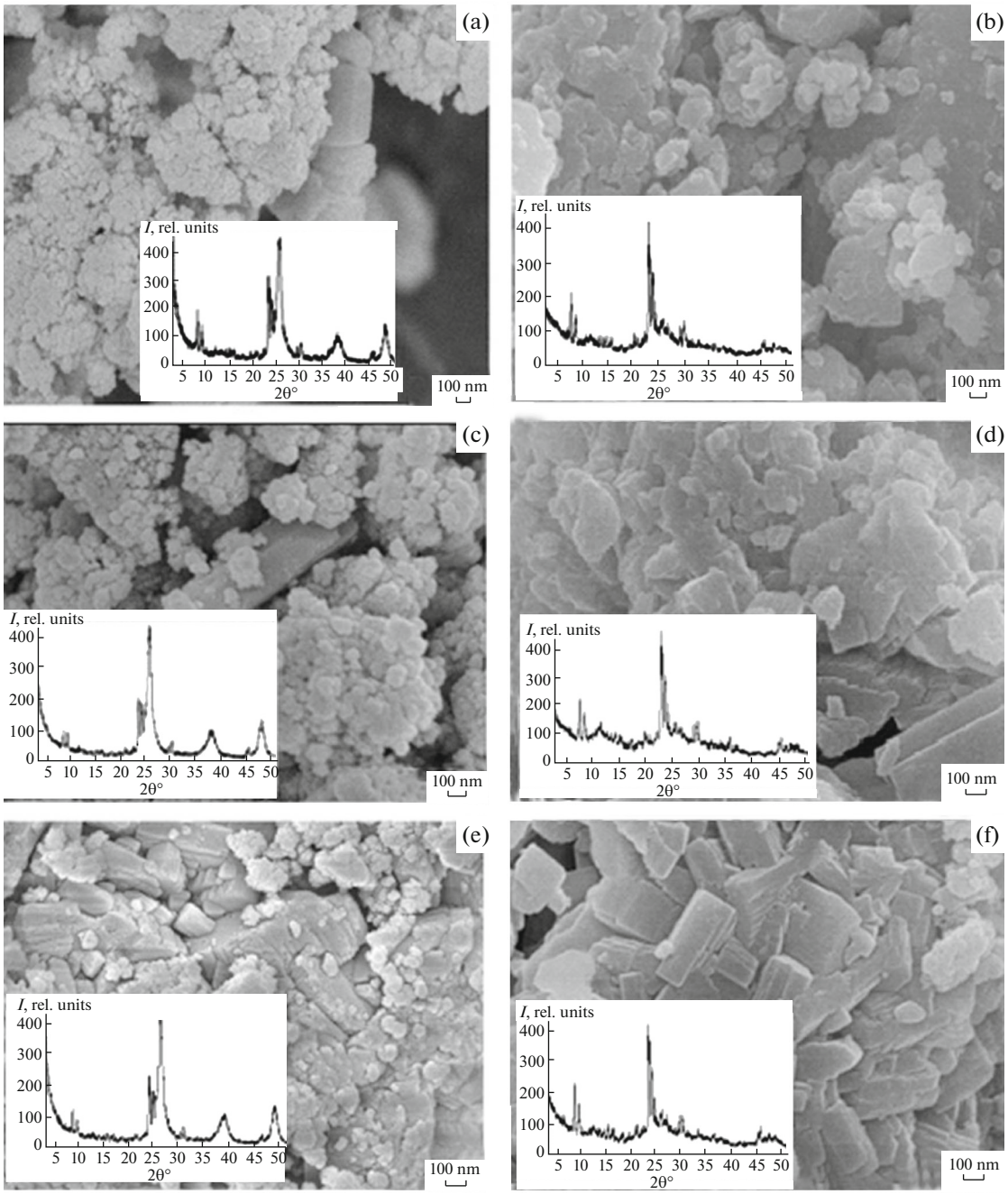

Fig. 10. Photographic images of the microstructures and diffractograms of the (a) Hombifine N/ZSM-5 (12) and (b) η-phase/ZSM-5 (12) zeolite nanocomposites prepared using the microwave treatment (method 1) of the (c) Hombifine N/ZSM-5 (12) and (d) η-phase/ZSM-5 (12) nanocomposites prepared using the ultrasound treatment and the (e) Hombifine N/ZSM-5 (12) and (f) η-phase/ZSM-5 (12) nanocomposites prepared without treatment.

composite samples in comparison with the nanocomposites on the basis of the η-phase, both in case of the synthesis without treatment (Figs. 10e, 10f) and with UST (Figs. 10c, 10d) and MWT (Figs. 10a, 10b); reduces the size of small spherical particles (<50 nm) in the case of MWT; and leads to the formation of larger fractions.

An analysis of the small-angle X-ray scattering (SAXS) curves (Fig. 11) shows that all the samples, both initial zeolites (Fig. 11a) and nanocomposites (Fig. 11c), are polydesperse (a Guinier zone is absent in them). The atomic-scattering background characteristic for the scattering on the polycrystalline objects is observed on the SAXS curves of zeolites (Fig. 11a)

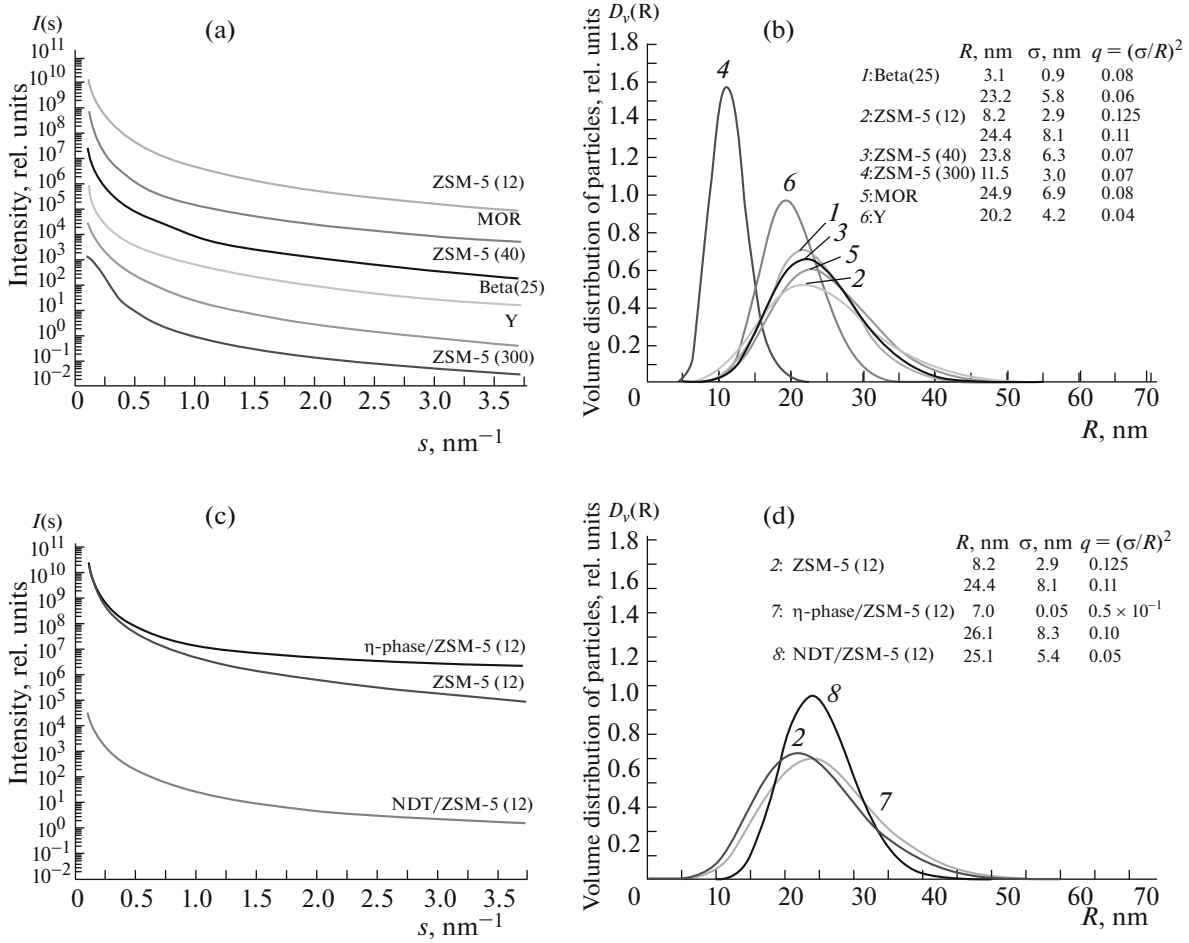

Fig. 11. Small-angle scattering curves (a) of different zeolites and (c) of the ZSM-5 zeolite and the η-phase/ZSM-5 (12) (MWT, method 1) and NTD/ZSM-5 (12) (method 2) nanocomposites; distribution curves of particles by their volume (with a spherical guess) (b) for different zeolites and (d) for the ZSM-5 zeolite, and the η-phase/ZSM-5 (12) (MWT, method 1) and NTD/ZSM-5 (12) (method 2) nanocomposites (<R> designates mean radii of scattering inhomogeneities, σ designates dispersions, and *q* is the polydispersity index).

and the NTD/ZSM-5 (12) and η-phase/ZSM-5 (12) nanocomposites (Fig. 11c). The most narrow size distribution of particles is revealed in the ZSM-5 (300) zeolite (Fig. 11b) and NTD/ZSM-5 (12) nanocomposite (Fig. 11d). For the Beta (25) and ZSM-5 (12) zeolites, and for the η-phase/ZSM-5 (12) (MWT) nanocomposite, smaller heterogeneities (pores) with mean radii of 3.1, 8.2, and 7 nm are found, in addition to the fraction with mean radii 23.2, 24.4, and 26.1 nm, respectively.

Method 2. In accordance with the diffractograms of the NTD/zeolite nanocomposites (Figs. 4–9), in which the NTD peaks are absent, it is supposed that NTD reacts with zeolites in these nanocomposites (Figs. 4d, 5d, 6e, 7d, 8e, 9d), except for the NTD/Y nanocomposite (Fig. 9d), in which NTD is present in an amorphous form. It should be noted that different kinds of interactions (at the level of microstructure or/and crystalline structure) between the zeolite and NTD are possible in the last case as well.

According to the SEM images (Fig. 12), the nanocomposite samples consist of spherical particles, with the exception of nanocomposites with MOR (Fig. 12o, NTD content is ~10 wt % according to X-ray spectral microanalysis) and Y (Fig. 12r, NTD content is 13.5 to 14.5 wt % according to X-ray spectral microanalysis), which have preserved faceted forms typical for the initial zeolites (Table 1). At the same time, the sizes of spherical particles in the nanocomposites with Beta (25) (Fig. 12c, $N_{SEM} \le 250$ nm with $N_{SEM(min)} \sim 35$ nm, NTD content is 1.8 to 29.6 wt %), ZSM-5 (12) (Fig. 12f, $N_{SEM} \le 300$ nm with $N_{SEM(min)} \sim 20$ nm, NTD content is up to 24.15 wt %), ZSM-5 (40) (Fig. 12i, fractal formations with $N_{SEM} \sim 250$ to 1700 nm comprised of the particles having a size from 60 to 160 nanometers with $N_{SEM(min)} \sim 25$ nm, NTD

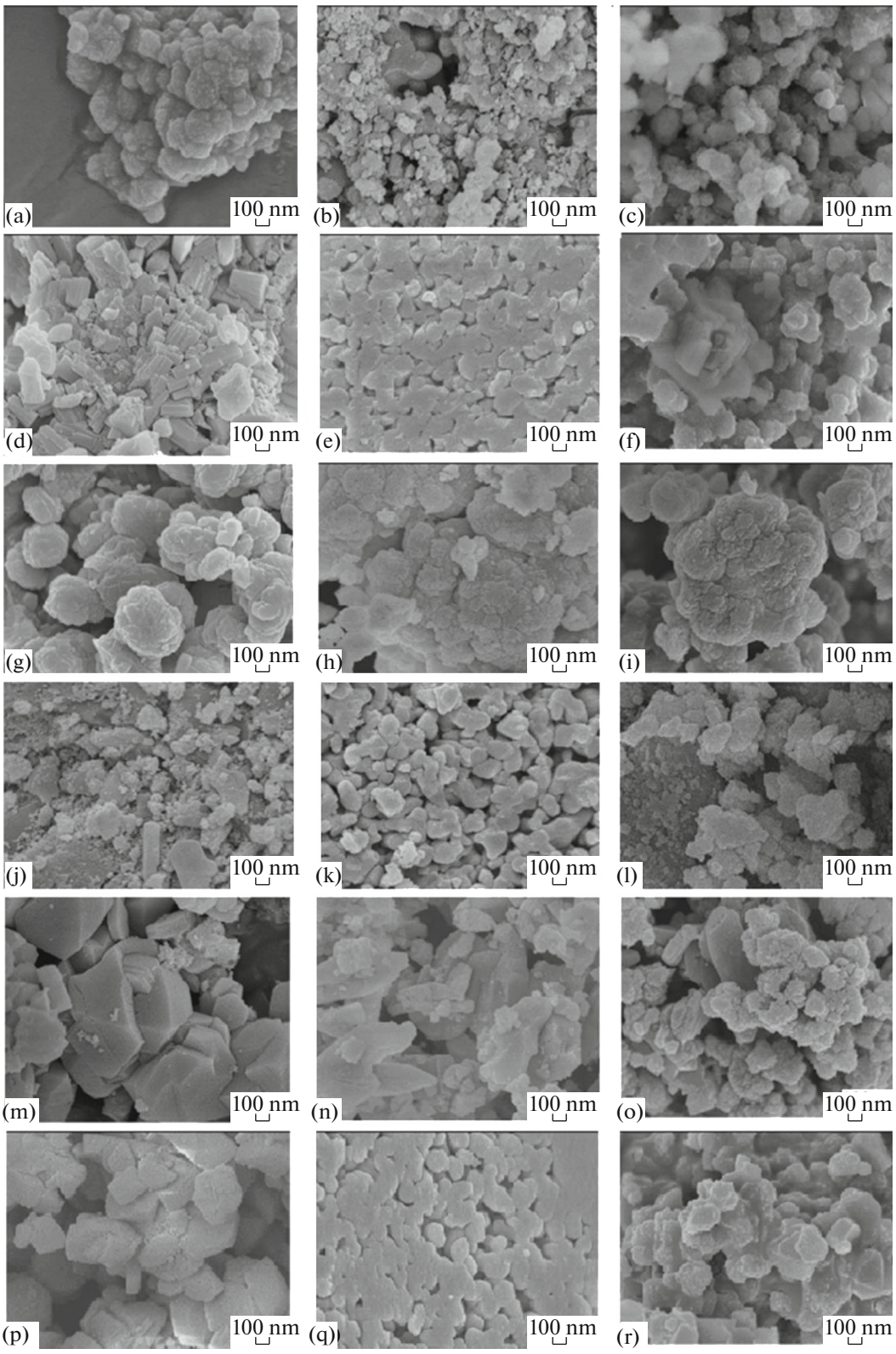

Fig. 12. Photographic images of the microstructures of the (a) Beta(25), (d) ZSM-5 (12), (g) ZSM-5 (40), (j) ZSM-5 (300), (m) MOR, and (p) Y zeolites, and of the (b) η-phase/Beta (25) (MWT, method 1), (c) NTD/Beta (25) (method 2), (e) η-phase/ZSM-5 (12) (MWT, method 1), (f) NTD/ZSM-5 (12) (method 2), (h) η-phase/ZSM-5 (40) (UST, method 1), (i) NTD/ZSM-5 (40) (method 2), (k) η-phase/ZSM-5 (300) (MWT, method 1), (l) NTD/ZSM-5 (300) (method 2), (n) η-phase/MOR (UST, method 1), (o) NTD/MOR (method 2), (q) η-phase/Y (MWT, method 1), and (r) NTD/Y (method 2) nanocomposites.

Table 3. Microstructure characteristics of the NTD/zeolite nanocomposites synthesized by method 2

Nanocomposite	BET method	t method	
	S_{BET}, m^2/g	$S_{micropore}$, m^2/g*	$S_{external}$, m^2/g**
NDT/Beta (25)	374.6	307.5	67.2
NDT/ZSM-5 (12)	322.3	190.4	131.9
NDT/ZSM-5 (40)	342.7	269.4	72.9
NDT/ZSM-5 (300)	293.0	110.3	182.7
NDT/MOR	48.7	10.8	37.9
NDT/Y	552.8	380.0	172.6

*Total surface area of all deep cracks and crinkles, pores open toward the surface.

**Total surface area of all particles with reckoning their roughness.

content is 3.2 to 7.8 wt %), ZSM-5 (300) (Fig. 12l, N_{SEM} ~ 50 to 600 nm with $N_{SEM(min)}$ ~ 20 nm, NTD content is up to 16.55 wt %), MOR (Fig. 12o, N_{SEM} ~ 100 to 500 nm with $N_{SEM(min)}$ ~ 25 nm), and Y (Fig. 12r, $N_{SEM} \le 300$ nm with $N_{SEM(min)}$ ~ 25 nm) exceed the comparable sizes in the η-phase/zeolite samples prepared by method 1 (Figs. 12n, 12q) and in the initial sample with the η-phase (N_{SEM} = 100 to 250 nm).

The synthesis of The NTD/ZSM-5(12) and NTD/Y nanocomposites synthesized by method 2 show an increase in the specific surface (to a greater extent for the NTD/ZSM-5 (12) nanocomposite) when compared with the matrix zeolites (Table 3). The specific surface decreases in the case of the remaining nanocomposites, most significantly for the NTD/MOR nanocomposite.

Adsorption Properties

Zeolites practically do not adsorb P(V), except for Y, which has the largest specific surface area according to our data (Table 1). The highest sorption ability among the samples with NTD is revealed for Hombifine N (Table 4), which has a larger specific surface area in comparison with the initial sample with the η-phase (Table 1).

The nanocomposites prepared by method 1 show adsorption properties only in the case of the Hombifine N/ZSM-5 (12) and Hombifine N/Y samples, and to a significantly lower extent when compared to the initial Hombifine N and Y zeolites (Table 4).

The nanocomposites synthesized by method 2 lead to an essential decrease in the concentration of P(V) ions in a standard aqueous solution; the largest value, $R_{P(V)}$ = 99.48%, is reached for the NTD/MOR system (Table 5). This is much higher than the sorption capacity of natural zeolite modified by La(III) ions ($R_{P(V)}$ ~ 90%) on the extraction of P(V) ions from aqueous systems [37].

It cannot be excluded that Si/Al silica modulus (5–12) exerts a stronger influence on the adsorption degree of P(V) by zeolites and nanocomposites on their basis rather than other physical and chemical characteristics of zeolites (Table 5). This does not contradict the earlier obtained results [38–42], according to which zeolites with a low value of Si/Al (from 1 to 3) show higher sorption capacity with reference to Pb(II), Cu(II), Ni(II), Co(II), and Zn(II) (natural zeolites) [38], to the Zn(II), Ni(II), Cd(II), Cu(II), and Co (II) cations (type A zeolites) [39], Cr(III), Ni(II), Zn(II), Cu(II), and Cd(II) (natural zeolites) [40], Co(II) (zeolites A and X) [41], and Cd(II) and Zn(II) (zeolites 4A, 13X, and bentonite) [42]. Upon a decrease in the silica modulus, the total concentration of the Bronsted acid centers increases due to the formation of protons for the conservation of the system

Table 4. Sorption degree (R, %) of initial components

Sample	R, %
Hombifine *N*	99.64
η-Phase	98.58
Beta (25)	1.59
ZSM-5 (12)	<1
ZSM-5 (40)	<1
ZSM-5 (300)	*
MOR	<1
Y	96.56

*Sorption ability is absent; maximum allowed concentration (MAC) of P(V) is 0.001% (R = 99.999%).

Table 5. Sorption degree of phosphorus (R_P, %) in the presence of the NTD/zeolite nanocomposites

Zeolite	Nanocomposite preparation method		
	Method 1		Method 2 NTD/zeolite
	η-phase/zeolite	Hombifine N/zeolite	
Beta (25)	*	*	99.08
ZSM-5 (12)	*	31.68	98.64
ZSM-5 (40)	**	**	98.95
ZSM-5 (300)	*	*	81.00
MOR	**	**	99.48
Y	*	14.12	98.07

*Sorption ability is absent.

**Adsorption properties were not studied.

electroneutrality, and that most likely determines the adsorption properties of the studied zeolites and nanocomposites on their basis.

On the other hand, the specific surface of the NTD/MOR nanocomposite is significantly decreased in comparison with the initial MOR zeolite, which is connected with the interaction (perhaps the adsorptive interaction) of NTD with MOR subsequently adsorbing P(V) ions. At the same time, a relationship between the sorption degree ($R_{P(V)}$, %) and the total surface area of all particles (Fig. 13, $S_{external,}$ m^2/g) is observed. Let us note that the interaction of the η-phase with zeolite in the case of the synthesis of nanocomposites by method 1 is supposed only for the nanocomposite on the basis of MOR.

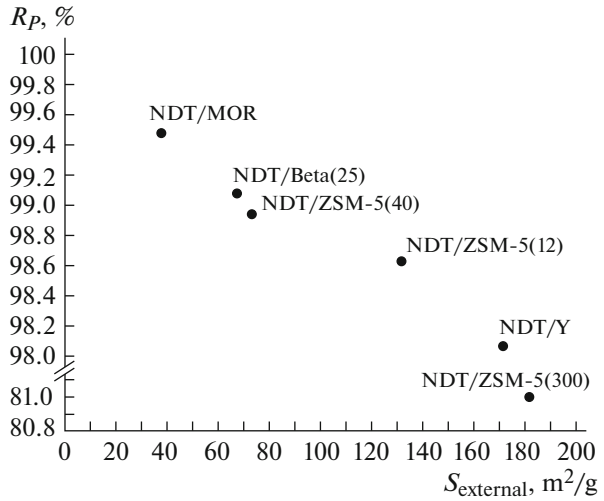

Fig. 13. Dependence of the sorption degree ($R_{P(V),}$%) on the total surface area of all particles ($S_{external,}$ m^2/g) for the NTD/zeolite nanocomposites prepared by method 2 (in situ).

CONCLUSIONS

As a result of our studies, NTD/zeolite nanocomposites are prepared for the first time by the in situ method and η-phase/zeolite and Hombifine N/zeolite nanocomposites with the Beta (25), ZSM-5 (12), ZSM-5 (40), ZSM-5 (300), MOR, and Y zeolites are obtained by the modified method of cold impregnation. It is established that the physicochemical properties (composition of nanoparticles, degree of amorphicity, size of crystallites and naoparticles, and specific surface area) of NTD and the characteristics of zeolites, as well as the method for the preparation of the NTD/zeolite nanocomposites, significantly affect the interaction of titanium dioxide nanoparticles with zeolites. It is found that the ultrasound or microwave treatment of the mixture of NTD and zeolite in the intermediate stage during the synthesis of nanocomposites leads to a decrease in the size of crystallites, an increase in the number of spherical formations when compared to the samples without treatment, and their aggregation into larger formations; however, the above effects are revealed to a greater extent in the case of MWT. It is demonstrated that the sizes of particles in the nanocomposite samples prepared by method 1 are comparable or smaller (in the case of the nanocomposites on the basis of MOR and Beta (25) with the η-phase) than the size of initial NTD, and smaller than the sizes of particles in the nanocomposites synthesized by method 2. It is revealed that the NTD/zeolite nanocomposites prepared by method 2 (in situ) show a high sorption capacity upon the extraction of P(V) ions from aqueous media. The highest degree of sorption is observed for the nanocomposite with MOR, which is determined by the strong interaction of NTD nanoparticles responsible for the adsorption properties with the initial zeolite.

ACKNOWLEDGMENTS

This work was supported by the Russian Foundation for Basic Research (grant no. 15-03-01289).

REFERENCES

1. A. A. Kubasov, "Ceolites in catalysis: today and tomorrow," Soros. Obrazov. Zh. **6** (6), 44–51 (2000).
2. N. Cioffi and M. Rai, Nano-Antimicrobials: Progress and Prospects (Springer Science & Business Media, 2012).
3. S. T. Yang, J. Kim, and W. S. Ahn, "CO_2 adsorption over ion-exchanged zeolite beta with alkali and alkaline earth metal ions," Microporous Mesoporous Mater. **135**, 90–94 (2010).
4. X. Xu, X. Zhao, L. Sun, and X. Liu, "Adsorption separation of carbon dioxide, methane, and nitrogen on Hb and Na-exchanged B-zeolite," J. Nat. Gas. Chem. **17**, 391 (2008).
5. A. I. Kryukov, A. V. Korzhak, G. M. Tel'biz, V. G. Il'in, and S. Ya. Kuchmii, "Photochemical and photocatalytic properties of zeolites containing titanium(IV) complexes and metallic palladium," Theor. Exp. Chem. **34**, 93–98 (1998).
6. M. Dadachov, "Novel titanium dioxide, process of making and method of using same," US Patent No. 2006/0171877 (2006).
7. M. Dadachov, "Novel adsorbents and process of making and using same," US Patent No. 2006/0144793 (2006).
8. S. Singh, K. C. Barick, and D. Bahadur, "Functional oxide nanomaterials and nanocomposites for the removal of heavy metals and dyes," Nanomater. Nanotechnol. **3**, 20:2013 (2013).
9. P. A. Demina, A. M. Zybinskii, G. M. Kuz'micheva, L. N. Obolenskaya, E. V. Savinkina, and N. A. Prokudina, "Adsorption ability of samples with nanoscale anatase to extract Nb(V) and Ta(V) ions from aqueous media," Crystallogr. Rep. **59**, 430 (2014).
10. G. M. Kuz'micheva, E. N. Domoroshchina, E. V. Savinkina, and L. N. Obolenskaya, "Nanosized titania with anatase etructure: sinthesis, characterization, applications and environmental effects," in *Titanium Dioxide* (Nova Science, 2014), Chap. 9, pp. 177–227.
11. P. A. Demina, A. A. Kuz'michev, A. M. Tsybinsky, L. N. Obolenskaya, G. M. Kuz'micheva, E. N. Domoroshchina, and E. V. Savinkina, "Synthesis, characterization and adsorption behavior of Mo(VI) and W(VI) ions on titanium dioxide nanoparticles containing anatase modification," Appl. Nanosci. **4** (8), 979–987 (2014).
12. S. Banerjee, S. C. Pillai, P. Falaras, K. E. O' Shea, J. A. Byrne, and D. D. Dionysiou, "New insights into the mechanism of visible light photocatalysis," J. Phys. Chem. Lett. **5**, 2543–2554 (2014).
13. O. Carp, C. L. Huisman, and A. Reller, "Photoinduced reactivity of titanium dioxide," Prog. Solid State Chem. **32**, 33–177 (2004).
14. Y. Matsumoto, U. Unal, N. Tanaka, A. Kudo, and H. Kato, "Electrochemical approach to evaluate the mechanism of photocatalytic water splitting on oxide photocatalysts," J. Solid State Chem. **177**, 4205–4212 (2004).
15. M. Padervand, M. R. Elahifard, R. V. Meidanshahi, S. Ghasemi, S. Haghighi, and M. R. Gholami, "Investigation of the antibacterial and photocatalytic properties of the zeolitic nanosized $AgBr/TiO_2$ composites," Mater. Sci. Semicond. Process. **15**, 73–79 (2012).
16. W. Zhang, F. Bi, Y. Yu, and H. He, "Phosphoric acid treating of ZSM-5 zeolite for the enhanced photocatalytic activity of TiO_2/HZSM-5," J. Mol. Catal. A: Chem. **372**, 6–12 (2013).
17. M. Takeuchi, T. Kimura, M. Hidaka, D. Rakhmawaty, and M. Anpo, "Photocatalytic oxidation of acetaldehyde with oxygen on TiO_2/ZSM-5 photocatalysts: effect of hydrophobicity of zeolites," J. Catal. **246**, 235–240 (2007).
18. M. Lafjah, F. Djafri, A. Bengueddach, N. Keller, and V. Keller, "Beta zeolite supported sol-gel TiO2 materials for gas phase photocatalytic applications," J. Hazard. Mater. **186**, 1218–1225 (2011).
19. M. N. Chong, Z. Y. Tneu, P. E. Poh, B. Jin, and R. Aryal, "Synthesis, characterisation and application of TiO_2-zeolite nanocomposites for the advanced treatment of industrial dye wastewater," J. Taiwan Inst. Chem. Eng., 1–9 (2014).
20. M. Takeuchi, J. Deguchi, M. Hidaka, Sh. Sakai, K. Woo, P-P. Choi, J-K. Park, and M. Anpo, "Enhancement of the photocatalytic reactivity of TiO_2 nano-particles by a simple mechanical blending with hydrophobic mordenite (MOR) zeolite," Appl. Catal. B: Environ. **89**, 406–410 (2009).
21. R. M. Mohamed, I. A. Mkhalid, M. Abdel Salam, and M. A. Barakat, "Zeolite Y from rice husk ash encapsulated with Ag-TiO2: characterization and applications for photocatalytic degradation catalysts," Desalinat. Water Treatm. **51**, 7562–7569 (2013).
22. Y.-H. Jan, L.-Y. Lin, M. Karthik, and H. Bai, "Titanium dioxide/zeolite catalytic adsorbent for the removal of NO and acetone vapors," J. Air Waste Manage. Assoc. **59**, 1186–1193 (2009).
23. A. Yasumori, S. Yanagida, and J. Sawada, "Preparation of a titania/X-zeolite/porous glass composite photocatalyst using hydrothermal and drop coating processes," Molecules **20**, 2349–2363 (2015).
24. M. P. Reddy, H. H. Phil, and M. Subrahmanyam, "Photocatalytic disinfection of Escherichia coli over titanium (IV) oxide supported on Hβ zeolite," Catal. Lett. **123**, 56–64 (2008).
25. A. B. Đukić, K. R. Kumrić, N. S. Vukelić, M. S. Dimitrijević, Z. D. Baščarević, S. V. Kurko, and L. L Matović, "Simultaneous removal of Pb^{2+}, Cu^{2+}, Zn^{2+} and Cd^{2+} from highly acidic solutions using mechanochemically synthesized montmorillonite-kaolinite/TiO_2 composite," Appl. Clay Sci. **103**, 20–27 (2015).
26. I. Jansson, S. Suarez, F. J. Garcia-Garcia, and B. Sanchez, "Zeolite-TiO_2 hybrid composites for degradation of pollutants in gas phase," in *Proceedings of the 8th European Meeting on Solar Chemistry and Photocatalysis: Environmental Applications. Greece, June 25–28, 2014,* pp. 320–321.
27. H. Li, M. L. Hu, and W. J. Zhang, "TiO_2 and 5A zeolite composite prepared for photocatalytic methyl orange

degradation," Adv. Mater. Res. **152–153**, 1129–1132 (2010).

28. L. N. Obolenskaya, M. A. Zaporozhets, G. M. Kuz'micheva, E. V. Savinkina, V. V. Podbel'skii, S. V. Amarantov, N. V. Sadovskaya, N. A. Prokudina, A. S. Avilov, and V. I. Nikolaichik, "Effect of methylene blue modification on the structural, morphological, and photocatalytic properties of nanosized η-TiO_2," Crystallogr. Rep. **60**, 406 (2015).
29. G. M. Kuz'micheva, A. A. Gainanova, and V. V. Podbel'skii, "Technol-1. Simulation of diffractograms of nanosized samples two-phase mixtures with TiO_2 with athanase and η-TiO_2 structure," State Registration Certificate of Software No. 2014660201 (2014).
30. O. Glatter and O. Kratky, *Small Angle X-Ray Scattering* (Academic, London, 1982).
31. T. C. Huang, H. Toraya, T. N. Blanton, and Y. Wu, "X-ray powder diffraction analysis of silver behenate, a possible low-angle diffraction standard," J. Appl. Crystallogr. **26**, 180–184 (1993).
32. L. N. Obolenskaya, G. M. Kuz'micheva, E. V. Savinkina, N. V. Sadovskaya, A. V. Zhilkina, N. A. Prokudina, and V. V. Chernyshev, "Influence of the conditions of the sulfate method on the characteristics of nanosized anatase-type samples," Russ. Chem. Bull. **61**, 2049 (2012).
33. S. Gregg and K. Sing, *Adsorption, Surface Area and Porosity* (Academic, New York, 1982).
34. A. S. Vyacheslavov, E. A. Pomerantseva, and E. A. Gudilin, "Measurement of surface area and porosity by the capillary nitrogen condensation method," Methodical Guide (2006).
35. G. M. Kuz'micheva, E. V. Savinkina, L. N. Obolenskaya, L. I. Belogorokhova, B. N. Mavrin, M. G. Chernobrovkin, and A. I. Belogorokhov, "Synthesis, characterization, and properties of nanoscale titanium dioxide modifications with anatase and η-TiO_2 structures," Crystallogr. Rep. **55**, 866 (2010).
36. I. Vasilyeva, G. Kuz'micheva, A. Pochtar, A. Gainanova, O. Timaeva, A. Dorokhov, and V. Podbel'skiy, "On the nature of the phase η-TiO_2," New J. Chem. (in press).
37. N. Ping, B. Hans-Jorg, L. Bing, L. Xiwu, and Z. Yong, "Phosphate removal from wastewater by model-La(III) zeolite adsorbents," J. Environ. Sci. **20**, 670–674 (2008).
38. W. Qiu and Y. Zheng, "Removal of lead, copper, nickel, cobalt, and zinc from water by a cancrinite-type zeolite synthesized from fly ash," Chem. Eng. J. **145** (3), 483–488 (2009).
39. H. Leinonen and J. Lehto, "Purification of metal finishing waste waters with zeolites and activated carbons," Waste Manage. Res. **19** (1), 45–57 (2001).
40. E. Álvarez-Ayuso, A. García-Sánchez, and X. Querol, "Purification of metal electroplating waste waters using zeolites," Water Res. **37** (20), 4855–4862 (2003).
41. H.-L. Chang and W.-H. Shih, "Synthesis of zeolites A and X from fly ashes and their ion-exchange behavior with cobalt ions," Ind. Eng. Chem. Res. **39** (11), 4185–4191 (2000).
42. G. Purna Chandra Rao, S. Satyaveni, A. Ramesh, K. Seshaiah, K. S. N. Murthy, and N. V. Choudary, "Sorption of cadmium and zinc from aqueous solutions by zeolite 4a, zeolite 13x and bentonite," J. Environ. Manage. **81** (3), 265–272 (2006).

Translated by O. Kadkin